

Experimental and computational investigation of the effect of Hsc70 structural variants on inhibiting amylin aggregation

Ali Chaari, Nabanita Saikia, Pradipta Paul, Mohammad Yousef, Feng Ding, Moncef Ladjimi

Item type

Journal Contribution

Terms of use

This work is licensed under a [CC BY 4.0](https://creativecommons.org/licenses/by/4.0/) license

This version is available at

https://manara.qnl.qa/articles/journal_contribution/Experimental_and_computational_investigation_of_the_effect_of_Hsc70_struct

Access the item on Manara for more information about usage details and recommended citation.

Posted on Manara – Qatar Research Repository on

2024-06-01



Experimental and computational investigation of the effect of Hsc70 structural variants on inhibiting amylin aggregation

Ali Chaari^{a,*}, Nabanita Saikia^{b,1}, Pradipta Paul^a, Mohammad Yousef^a, Feng Ding^b, Moncef Ladjimi^a

^a Weill Cornell Medicine–Qatar, Qatar Foundation–Education City, P.O. Box 24144, Doha, Qatar

^b Department of Physics and Astronomy, Clemson University, Clemson, SC 29634, USA

ARTICLE INFO

Keywords:
Amylin
Chaperone
Amyloid
Diabetes

ABSTRACT

The misfolding and aggregation of human islet amyloid polypeptide (hIAPP), also known as amylin, have been implicated in the pathogenesis of type 2 diabetes (T2D). Heat shock proteins, specifically, heat shock cognate 70 (Hsc70), are molecular chaperones that protect against hIAPP misfolding and inhibits its aggregation. Nevertheless, there is an incomplete understanding of the mechanistic interactions between Hsc70 domains and hIAPP, thus limiting their potential therapeutic role in diabetes. This study investigates the inhibitory capacities of different Hsc70 variants, aiming to identify the structural determinants that strike a balance between efficacy and cytotoxicity. Our experimental findings demonstrate that the ATPase activity of Hsc70 is not a pivotal factor for inhibiting hIAPP misfolding. We underscore the significance of the C-terminal substrate-binding domain of Hsc70 in inhibiting hIAPP aggregation, emphasizing that the removal of the lid subdomain diminishes the inhibitory effect of Hsc70. Additionally, we employed atomistic discrete molecular dynamics simulations to gain deeper insights into the interaction between Hsc70 variants and hIAPP. Integrating both experimental and computational findings, we propose a mechanism by which Hsc70's interaction with hIAPP monomers disrupts protein-protein connections, primarily by shielding the β -sheet edges of the Hsc70- β -sandwich. The distinctive conformational dynamics of the alpha helices of Hsc70 potentially enhance hIAPP binding by obstructing the exposed edges of the β -sandwich, particularly at the $\beta 5$ - $\beta 8$ region along the alpha helix interface. This, in turn, inhibits fibril growth, and similar results were observed following hIAPP dimerization. Overall, this study elucidates the structural intricacies of Hsc70 crucial for impeding hIAPP aggregation, improving our understanding of the potential anti-aggregative properties of molecular chaperones in diabetes treatment.

1. Introduction

The International Diabetes Federation reported that 537 million (10.5%) adults aged 20–79 years lived with diabetes in 2021, a figure which is expected to rise to 783 million (12.2%) by 2045 [1]. Type 2 diabetes (T2D) accounts for 90% of all diabetes and is characterized by hyperglycemia and insulin resistance secondary to pancreatic β -cell dysfunction, gradual reduction in insulin secretion, and loss of β -cell mass [2]. Although insulin is widely associated with the expression of diabetes, a second hormone, human islet amyloid polypeptide (hIAPP; also called amylin), seems to be also involved [3]. In fact, post mortem studies of over 90% of T2D patients revealed the presence of deposits of extracellular hIAPP aggregates in their pancreas [4–6]. hIAPP is co-

secreted with insulin in a molar ratio of $\sim 1:100$ from pancreatic β -cells, playing important roles in the regulation of body glucose levels [7]. Chronic hyperglycemia such as that in diabetes is characterized by an increase in the hIAPP to insulin ratio leading to a greater probability of local aggregation in the β -cell periphery post-release [8]. hIAPP aggregation and amyloid formation contributes to T2D pathophysiology by causing β -cell loss and apoptosis [9,10].

The 3-exon gene encoding hIAPP on chromosome 12 first expresses an 89-amino acid pre-pro-peptide that subsequently forms a 67-amino acid pro-peptide (proIAPP) following N-terminal cleavage of a 22-amino acid signal peptide [7,11]. Following post-translational changes in the endoplasmic reticulum and Golgi complex, the active 37-amino acid peptide hormone known as hIAPP is expressed [7,12]. This

* Corresponding author.

E-mail address: alc2033@qatar-med.cornell.edu (A. Chaari).

¹ Present address: Chemistry Department, Ivan Hilton Science Center, New Mexico Highlands University, Las Vegas, NM 87701, USA

<https://doi.org/10.1016/j.bpc.2024.107235>

Received 6 January 2024; Received in revised form 3 April 2024; Accepted 3 April 2024

Available online 9 April 2024

0301-4622/© 2024 The Author(s). Published by Elsevier B.V. This is an open access article under the CC BY license (<http://creativecommons.org/licenses/by/4.0/>).

peptide is characterized by its low solubility and high propensity to form aggregates and amyloid fibrils via a multistep nucleation-dependent process [13]. In solution it has been reported that hIAPP aggregation involves a primary and secondary nucleation and highlighted the importance of secondary nucleation in fibril formation [14,15]. This was explained by the fact that hIAPP possess particular residues or regions called amyloidogenic regions that lead to the formation of beta-sheet domains involved in the aggregation processes [16–19]. Although many studies indicated that residues 20–29 play a critical role in hIAPP fibril formation [17,18,20], other reports reported that the above-mentioned sequence is not the sole amyloidogenic determinant [16,21]. In one study, residues 25–29 corresponding to Ala-Ile-Leu-Ser-Ser demonstrated significant amyloidogenic propensity, while substitution of serine at position 28 with proline, a modification observed in various rodent species, notably suppressed the formation of amyloid fibrils to a large extent [18].

In vivo, it has been shown that the aggregation mechanism of hIAPP in the presence of membranes may lead to membrane dysfunction [22]. In fact, negatively charged lipids have been shown to enhance hIAPP fibrillation, a process that occurs through a nucleated growth mechanism, and dominated by secondary nucleation events, which occur at the interface between existing fibrils and the membrane surface [22–24]. hIAPP aggregation affects physiological mechanisms in the maintenance of cellular homeostasis and contributes to pancreatic β -cell failure and death [25]. Some mechanisms that have been proposed and investigated in literature include hIAPP oligomer-induced endoplasmic reticulum stress and subsequent impaired unfolded protein response [26], overwhelming the ubiquitin/proteasome system protein quality control system secondary to ubiquitin carboxyl terminal hydrolase L1 insufficiency leading to accumulation of polyubiquitinated proteins [27], with further contribution of extracellular hIAPP amyloidogenesis on the abovementioned intracellular events [28], hIAPP oligomer-induced disruption of autophagosomal and lysosomal membranes [29], IL-1 β -mediated inflammation leading to impaired β -cell function, and the recently described role of thioredoxin-interacting protein in loss of β -cell mass [30,31].

Using human IAPP transgenic rat models, Matveyenko and Butler investigated the relationship between prospective changes in islet morphology and insulin secretion and showed that hIAPP-induced beta-cell apoptosis triggers deficiencies in insulin secretion and beta-cell mass, leading initially to hepatic insulin resistance and impaired fasting glucose, followed by peripheral insulin resistance, hyperglucagonemia, and diabetes [32]. These observations have also been reproduced in human studies [10], highlighting that hIAPP-induced beta-cell loss may play an important role in the etiopathogenesis of T2D, especially given that studies have reported a strong inverse correlation between β -cell area and amyloid deposition [9].

Beside the pancreas, hIAPP amyloid aggregates have also been reported in various other organs of clinical significance in T2D patients [11]. Amylin oligomers and plaques were reported to be present in the grey matter of diabetic patients with dementia, with further substantial amylin deposition in both blood vessels and perivascular spaces [33]. Despite no evidence of amylin synthesis in the brain, amylin amyloid buildup in cerebral blood vessels may hinder A β clearance, contributing to dementia pathogenesis [34]. Other studies have identified amylin amyloid deposition as a risk for brain endothelial dysfunction, precipitating stroke [35]. One study reported that nearly half of all patients with diabetic nephropathy have amylin deposition and that this was directly associated with disease severity [36]. hIAPP has also been reported to deposit in the blood, heart and eyes of diabetic patients [11]; further research in this field is ongoing.

Molecular chaperones, such as heat shock proteins (Hsps), are known to protect cells against the toxic accumulation of misfolded proteins that form under normal and stressful environments and maintain protein homeostasis [37]. Along with proteases, heat shock proteins form the first defense line to nullify cytotoxicity by refolding and degrading

misfolded proteins. The constitutive (Hsc70) and inducible (Hsp70) are two forms of the 70 kDa cytosolic heat shock protein chaperones (Hsp70s) that inhibit aggregation of misfolded proteins in amyloid diseases [38]. Recently, it was reported that Hsp70 inhibits hIAPP aggregation by binding strongly to the heterogeneous prenucleation oligomers (but poorly with monomers) thus preventing nucleation of hIAPP in sub-stoichiometric concentrations, even in the absence of ATP and co-chaperones [39].

Hsc70, the constitutive form of Hsp70, consists of an N-terminal ATPase-nucleotide-binding domain (NBD) and a C-terminal substrate binding domain (SBD) containing the canonical binding cleft for misfolded proteins [40]. The SBD consists of a peptide binding subdomain (PBSD), also known as substrate binding pocket, an α -helical subdomain comprising of five helices, namely α A, α B, α C, α D, and α E that help stabilize the binding of chaperone to target proteins, and lastly, an EEVD motif that binds to other co-chaperones and Hsps. Hsp70 attenuates protein misfolding via two well-known mechanisms: ATP-dependent “foldase” activity that helps refold the misfolded proteins back to their native conformation and the ATP-independent “holdase” function that binds to the misfolded proteins and prevents their aggregation to oligomeric species [41]. It is debatable, however, whether the holdase function protects cells by preventing aggregation or exacerbates neurotoxicity by stabilizing harmful oligomers.

In this study, we investigate the inhibitory potential of various Hsc70 variants on hIAPP aggregation to identify the chaperone variant with the least cytotoxicity yet optimal activity via both in vitro and in silico methodologies and propose a general mechanism for their interaction.

2. Material and methods

2.1. Expression and purification of Hsc70 and its structural domains

Hsc70 and its different structural domains (Figs. 1A and B) were cloned into a Pet14 vector, overexpressed in BL21 pLysS E.coli and purified as described previously [41–44]. The purified proteins (in PBS buffer: 1.5 mM KH₂PO₄, 150 mM NaCl, 3 mM KCl and 8 mM Na₂HPO₄) were concentrated by Millipore Centricon, dialyzed against 50 mM Tris-HCl (pH 7.4), 150 mM KCl, filtered through a sterile 0.22 μ m pore size filter and stored at -20°C . Before the use of Hsc70 or any of its structural domains, the purity of these proteins was analyzed by SDS-PAGE (Fig. S1). To determine the molecular mass of the native protein and check the aggregation states, we analyzed the purified samples with high performance liquid chromatography (HPLC) using a superdex 70 column previously equilibrated with 5 mM phosphate buffer (pH 7.4) with a flow rate of 0.5 mL/min (Fig. S1). Finally, protein concentrations were determined photometrically using the Lowry procedure [45]. The activity of Hsc70 was analyzed using a luciferase refolding assay as described by Pemberton et al. [46].

2.2. hIAPP aggregation protocol

Stock solution of hIAPP (1 mM) was prepared in 100% HFIP and stored at -20°C as described in a previous work [47]. Before starting the aggregation, aliquots of hIAPP peptide were filtered through a 0.22 μ m filter from the stock solution and freeze dried. 15 μ M of hIAPP was prepared in 50 mM Tris HCl buffer (pH 7.4) and aliquots of hIAPP were prepared in the presence or absence of Hsc70 and its structural domains at different concentrations. The prepared solutions were incubated under the physiological conditions (pH 7.4 and at 37°C) to allow amyloid fibril formation. Samples were incubated for 36 h. Different aliquots were taken at different times for the different analysis.

2.3. Thioflavin T (ThT) fluorescence assay

hIAPP fibril formation was monitored by characteristic changes in the Thioflavin T (ThT) fluorescence intensity. Samples co-incubated

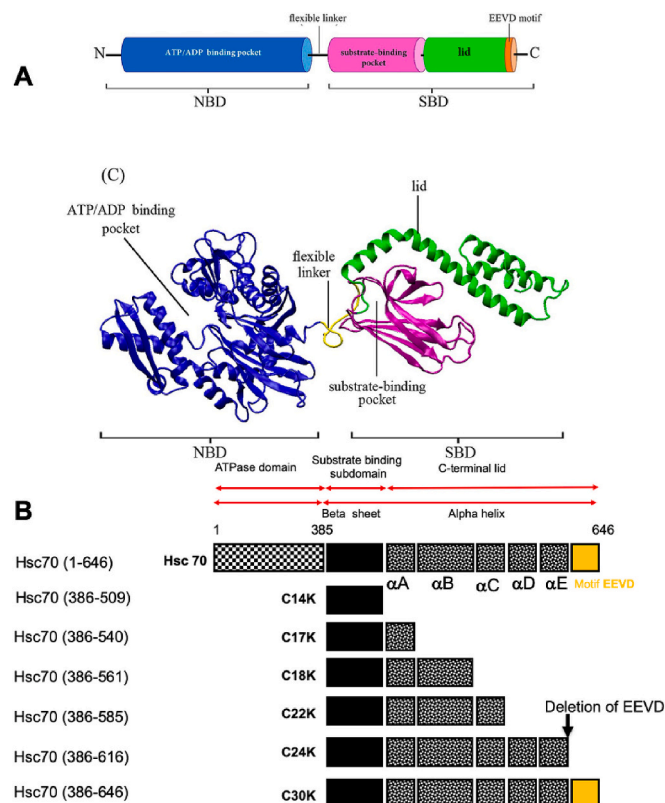


Fig. 1. Representation of Hsc70 and its respective structural domains.
A: The Hsp70s schematic domains are based on the E.coli Hsp70 homologue, DnaK. This chaperone is made of two structural and functional domains: An N-terminal ATPase domain and a C-terminal peptide-binding domain (residues 386–646) involved in unfolded protein binding. The C-terminal domain is in turn composed of 2 subdomains: the peptide-binding subdomain (PBSD) per se (residues 386–509) and the C-terminal α -helical subdomain (residues 510–646) that plays the role of a lid (composed of 5 helices) that regulates substrate binding and release under the control of ATP binding and hydrolysis. Also, at the end of the C-terminal, an EEVD motif participates in binding to co-chaperones and other Hsp's.
B: Schematic representation of Hsc70 and its structural domains used in the current study.

without or with Hsc70 and their structural domains were diluted 25-fold with ThT solution (15 μ M). ThT fluorescence measurements were performed in a 50 μ L quartz black cuvette using Perkin Elmer model LS 55 without shaking and at room temperature (25 $^{\circ}$ C). An excitation filter of 440 nm and an emission filter of 480 nm were used [47]. The emission and excitation slits were set to 5 nm and a 1 cm cuvette was used for all experiments. Nonspecific background fluorescence was subtracted from the samples by using appropriate blanks in the absence of proteins. Each experiment was performed in triplicate and a median was represented and the time-dependence of ThT fluorescence will be fitted to a sigmoidal growth model using:

$$Y = y_i + m_i x + \frac{y_f + m_f x}{1 + \exp\left(-\left[\frac{(x-x_0)}{\tau}\right]\right)}$$

where Y is the intensity of fluorescence at different times, x is the incubation time, y_i and y_f are the maximal and minimal fluorescence intensity, x_0 is the incubation time when we have 50% of the maximal of fluorescence, τ is the inverse of the apparent constant of growth K_{app} and m_i , m_f the adjustment parameters. The lag time t is described by $t_{lag} = x_0 - 2\tau$.

2.4. Aggregation of hIAPP observed at increasing concentration of Hsc70 by ThT assay

Concentration-effect data from the ThT fluorescence assays were fitted to a sigmoidal function using the Prism 6.0 software package, to extract the relevant inhibition parameters using the equation:

$$F = F_{min} + [F_{max} - F_{min}] / [1 + 10^{(log IC_{50} - log x)/n}]$$

Where F is the fluorescence quantum yield of ThT in the presence of Hsc70 at concentration x , F_{\max} and F_{\min} represent the maximum and minimum of the fluorescence quantum yield of ThT in the absence and presence of inhibitors, respectively. The values of the parameters, n (Hill coefficient) and IC_{50} (the concentration of inhibitor that results in 50% of maximal inhibition) were determined by fitting the experimental data by non-linear least-square method.

2.5. Cell viability assay

Pancreatic INS-1E cells which show a high resemblance with native β -cells, were used [48]. The cells were cultured in RPMI 1640 medium (with 2 mM glutamine) supplemented with 5% fetal calf serum, 10 mM HEPES, pH 7.4, 1 mM sodium pyruvate, 50 μ M 2-mercaptoethanol, 100 units/mL penicillin and 0.1 mg/mL streptomycin, at 37 $^{\circ}$ C, 5% CO₂, pH 7.4. Drug treatments were usually done 24 h after seeding the cells [49]. The cells were cultured then seeded into 96-well plates and grown for 24 h prior to exposure to different intermediates of hIAPP or a mixture of hIAPP with different Hsc70 proteins. Samples of hIAPP solutions with and without chaperones were initially diluted in the culture medium and then added to the cells to achieve the required final concentrations. Treated cells with amyloid incubation buffer were used as control.

The toxicity of hIAPP aggregate co-incubated without or with Hsc70 and its structural domains were assessed by the MTT reduction assay (3-(4,5-dimethylthazol-2-yl)-2,5-diphenyltetrazolium bromide), as previously reported [41]. In our experiments, MTT were added in triplicate to cells to have a final concentration of 1 mg/mL. After that, cells were incubated for 2 h before removing the cell culture medium containing MTT. Finally, a buffer containing 25 μ l of 0.1 M glycine, 0.1 M NaCl (pH 10.5) and 200 μ l of DMSO (Sigma) was added per well and absorbance will be measured at 550 nm. This experiment was repeated 3 times and treated cells with amyloid incubation buffer were used as control.

2.6. Discrete molecular dynamic simulations

Discrete Molecular Dynamic (DMD) simulations are a rapid and predictive event-driven molecular dynamics algorithm that utilizes discrete, distance-based stepwise potentials, rather than continuous potentials to mimic constraints [50]. DMD has been extensively employed to study protein folding and aggregation, conformational dynamics of intrinsically disordered proteins, and the supertertiary structure of proteins [51–55]. A detailed discussion of the DMD algorithm can be found elsewhere [56,57]. Briefly, in DMD, the atoms move with constant velocities between collision events until the potential between two atoms becomes discontinuous. At this point, the motion of atoms is immediately recalculated by solving the ballistic equations of motion that consider the principles of energy, momentum, and angular momentum conservation. To improve computational speed and increase sampling efficiency, DMD uses a quicksort algorithm to identify colliding atoms and only updates the velocities of those atoms participating in the collision, instead of solving Newton’s equations of motion for every atom in the system.

The sequence of Hsc70 chaperone protein was adopted from UniProt (Entry: P11142). Three truncated domains of Hsc70 were considered: Hsc70- β -sandwich (385-509aa), Hsc70 + helixA (385-540aa), and Hsc70 + α -helices (385-615aa). To study the binding of hIAPP peptides with Hsc70 chaperone and the effect of Hsc70 on the inhibition

of hIAPP peptide aggregation, we considered the monomer and dimer of hIAPP peptide. The initial structure of hIAPP used in our simulation was taken from the protein data bank (PDB ID: 2L86). In the present study, 20 independent DMD simulations, each lasting 700 ns, were performed for each system, starting with different initial states (coordinates, orientations, and velocities). Initially, the hIAPP peptides were placed randomly in the periodic simulation box of dimensions $125 \times 125 \times 125 \text{ \AA}^3$. The initial separation in the intermolecular distance between hIAPP peptides and Hsc70 variants was 15 \AA . The Medusa force field was used in all-atom DMD to describe the nonbonded interatomic interactions, namely van der Waals (vdW), solvation, hydrogen bonding, and electrostatics. The vdW parameters were adopted from the CHARMM19 united-atom force field, and the distance and angular-dependent hydrogen bonds are explicitly modeled by a reaction-like algorithm. The inter-atomic interactions were modeled by stepwise functions

mimicking the continuous potential functions. The solvation effects were implicitly modeled by the EEF1 implicit solvation model [58]. The hydrogen bond interactions were depicted by a reaction-like algorithm. Screened electrostatic interactions were modeled by the Debye–Hückel approximation with the Debye length set as 10 \AA , corresponding to 100 mM of NaCl under physiological conditions. The units of mass, time, length, and energy were 1 Da, ~ 50 femtoseconds, 1 \AA , and 1 kcal/mol, respectively. The temperature of the system was maintained at 300 K using the Anderson's thermostat. The DMD program is available free of charge to academic users via Molecules in Action, LLC (<http://moleculesinaction.com>).

2.7. Computational analysis

Secondary structure analyses utilized the dictionary secondary

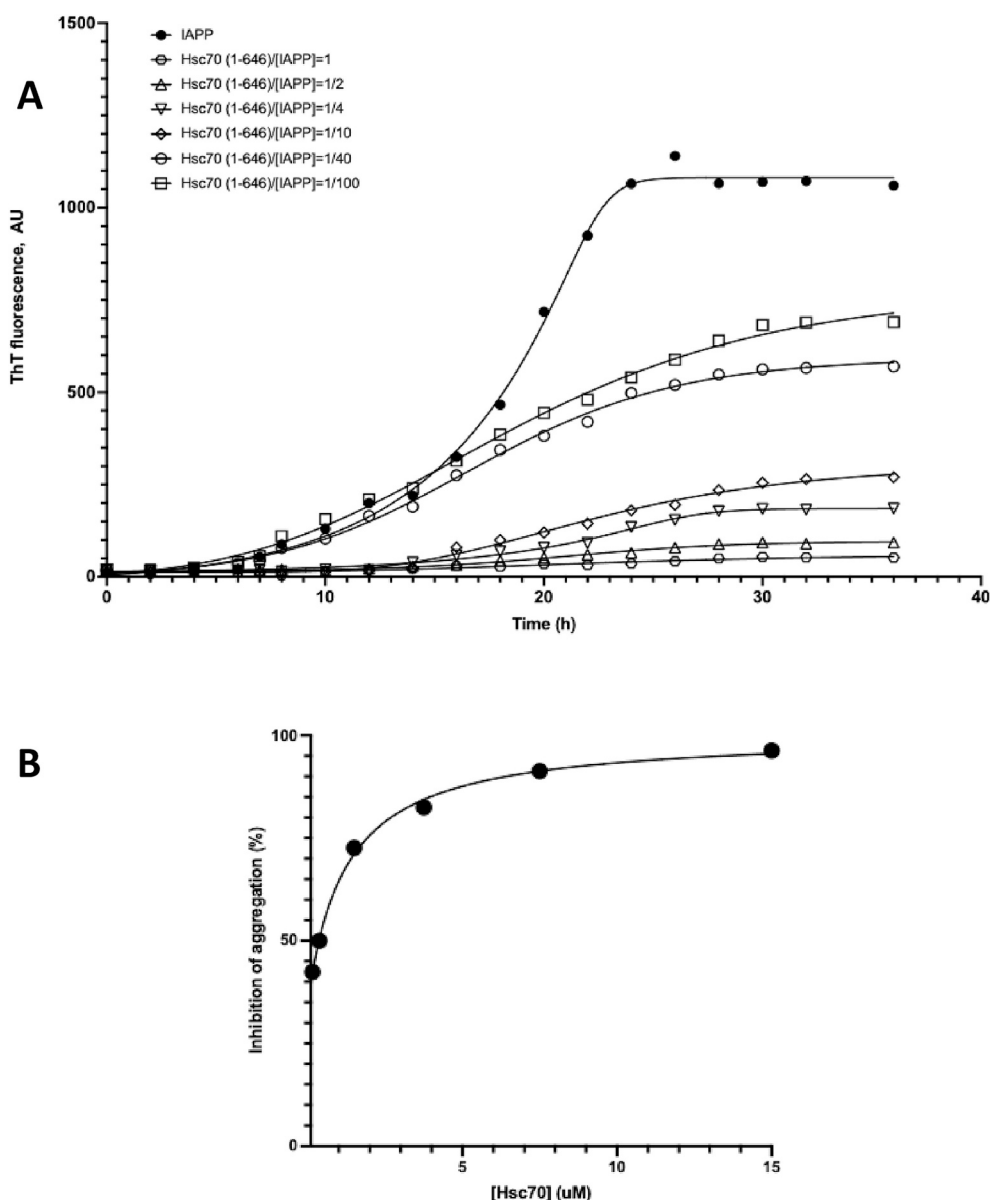


Fig. 2. Analysis of hIAPP aggregation in the absence and presence of Hsc70.

A: Time course of hIAPP (15 μM) aggregation monitored by ThT fluorescence in the absence and presence of increasing amounts of Hsc70. The time dependence of ThT fluorescence was fitted to a sigmoidal growth model.

B: Percentage of Inhibition of hIAPP aggregation at increasing concentrations of [Hsc70]. This % of inhibition was calculated at 36 h taking the fluorescence of hIAPP in the absence of Hsc70 as 0% of aggregation. The percentage of inhibition of for each assay is calculated based on the plateau signal at 36 h using the GraphPad Prism nonlinear regression model for dose-response (three parameters).

structure of protein (DSSP) method described by Kabsch and Sander [59]. A hydrogen bond was formed if the distance between backbone N and O atoms was ≤ 3.5 Å and the angle of $N-H\cdots O \geq 120^\circ$. Inter-chain peptide interactions were analyzed by the residue-residue contact frequency. Here, a pairwise residue contact was defined when the distance between the heavy atoms of two non-sequential residues was < 0.55 nm. The binding probability and number of interchain H-bonds between hIAPP and Hsc70 along the two exposed β -strand edges ($\beta 2 + \beta 3$ and $\beta 5 + \beta 8$ strands) of the β -sandwich were computed for each of the systems.

3. Results and discussion

3.1. Hsc70 inhibits hIAPP aggregation in a concentration-dependent manner

Given that the oligomers are believed to be the primary pathologic species [60–62], we investigated the effect of Hsc70's on hIAPP aggregation using ThT fluorescence (Fig. 2A). The results indicate that as Hsc70 concentration increases, there is a corresponding decrease in ThT fluorescence, suggesting that the inhibitory capability of Hsc70 depends on its concentration. Even when Hsc70 is present in sub-stoichiometric concentrations (0.15, 0.375, 1.5, 3.75 and 7.5 μ M), it still delays the aggregation kinetics of Hsc70. An inhibitory effect from Hsc70 (1–646) can be seen at concentrations as low as 1/100 compared to hIAPP (42%). The maximum inhibition (96%) is observed when the ratio of [Hsc70] to [hIAPP] is 1 (Fig. 2A). Additionally, the length of the lag phase, before hIAPP starts aggregating increases with increasing Hsc70 levels. For instance, this lag time nearly doubles when Hsc70 is introduced, suggesting Hsc70 (1–646) hampers the hIAPP aggregation process (Fig. 2A). Furthermore, the results show that IC_{50} in Hsc70's presence is 1.3 μ M, and close to complete aggregation is seen with 15 μ M of Hsc70 (Fig. 2B).

3.2. The ATPase activity of Hsc70 is not required for inhibiting the aggregation of hIAPP

The C-terminal domain of Hsp70/Hsc70 is known to engage target proteins and peptides due to its peptide-binding site [60]. Conversely, the N-terminal ATPase binding domain is not directly associated with target protein binding but influences peptide binding [60,63]. Contrary to prior understanding, ATPase activity in Hsc70, Hsp70, or Hsp90 was not essential to prevent the aggregation of amyloid proteins like α -synuclein. [41,64–66] Our study aimed to discern the role of the N-terminal ATPase binding domain in inhibiting hIAPP aggregation. To elucidate the role of various nucleotide-bound states during the ATPase cycle, aggregation tests were conducted in the absence or presence of ATP, ADP, or AMPPNP (a non-hydrolyzable ATP analog) as depicted in Fig. 3. The ThT fluorescence results revealed that Hsc70 loaded with any of these three nucleotides did not affect hIAPP aggregation when compared to its absence indicating that the N-terminal domain of Hsc70 was not essential for inhibition of hIAPP aggregation (Fig. 3A). Moreover, Fig. 3B shows that the SBD alone, consisting of residues 386–646, was equally efficient at inhibiting aggregation as the full-length Hsc70 protein. These data align with the “holdase” mechanism of Hsc70, refuting the “foldase” mechanism that necessitates the catalytic domain. As such, the SBD domain of Hsc70 (386–646) can effectively sequester hIAPP monomers, hindering their aggregation or fibril formation. Recently, it was also shown that Hsp70 SBD domain can block α -synuclein oligomerization in an ATP-independent holdase model without input from the NBD [40].

3.3. Structural domains of Hsc70 enhance its chaperone activity for hIAPP

As highlighted earlier, previous studies have indicated that the C-terminal domain of Hsc70 is essential for peptide and target protein binding due to its inclusion of the peptide-binding site [41,64–66]. To

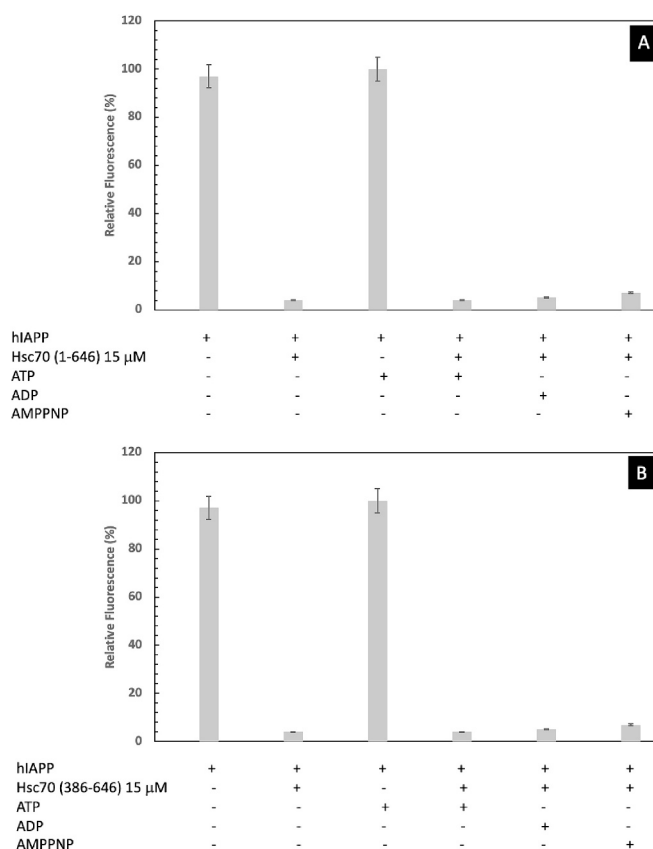


Fig. 3. Effect of nucleotides and a competing peptide on the modulation of hIAPP aggregation by Hsc70. Bar diagram representing the relative ThT levels reached at the end of the aggregation reaction. 15 μ M of hIAPP with or without A: full-length Hsc70 (1–646), B: Hsc70 (386–646), and ATP, ADP, or AMPPNP, a non-hydrolyzable ATP analog were included in the reaction mixture where indicated. Error bars denote one s.d. from the mean, calculated from three independent experiments.

pinpoint the regions of the C-terminal domain of Hsc70 crucial for inhibiting hIAPP aggregation, we evaluated the activity of its distinct structural sub-domains. Specifically, the C-terminal domain of Hsc70 comprises two sub-domains: a PBS (residues 386–509), which is exclusively composed of β -sheets, and a lid subdomain (residues 510–646) consisting entirely of α -helices (Fig. 1) [67,68]. In this study, our emphasis was on eliminating those parts of Hsc70 known to function as lids, locking target peptide ligands into the chaperone's binding site, as well as removing the EEVD sequence. This sequence is recognized for facilitating the interaction of Hsp70 or Hsc70 with Hsp90, aiding in refolding, and with CHIP, directing proteasomal degradation [40,69].

The results show that the PBS, devoid of the Hsc70 lid subdomain, can inhibit hIAPP aggregation (with 32% inhibition at a [Hsc70]/[hIAPP] ratio of 1/10, Fig. 4A). However, its efficiency is substantially lower than the complete C-terminal domain, inclusive of the Hsc70 lid (residues 386–646), which inhibits 88% at the same ratio. Intriguingly, the inhibition effect of the C-terminal with the lid subdomain (residues 386–646) mirrors that of the entire Hsc70, as illustrated in Fig. 4A and detailed in Table 1. Removing the C-terminal EEVD residues from Hsc70 (residues 386–616) doesn't impede its ability to inhibit hIAPP aggregation, suggesting that this known site for protein-protein interaction isn't involved in the detected inhibition.

Further, the dissociation constant (K_d) for the PBS binding to hIAPP was found to be 0.872 μ M, over three times the K_d of the intact C-terminal domain of Hsc70 (0.256 μ M) as shown in Table 1 and Fig. 4B. This suggests that the lid subdomain reinforces the binding stability of hIAPP to the chaperone. This is supported by the fact that the K_d for the entire

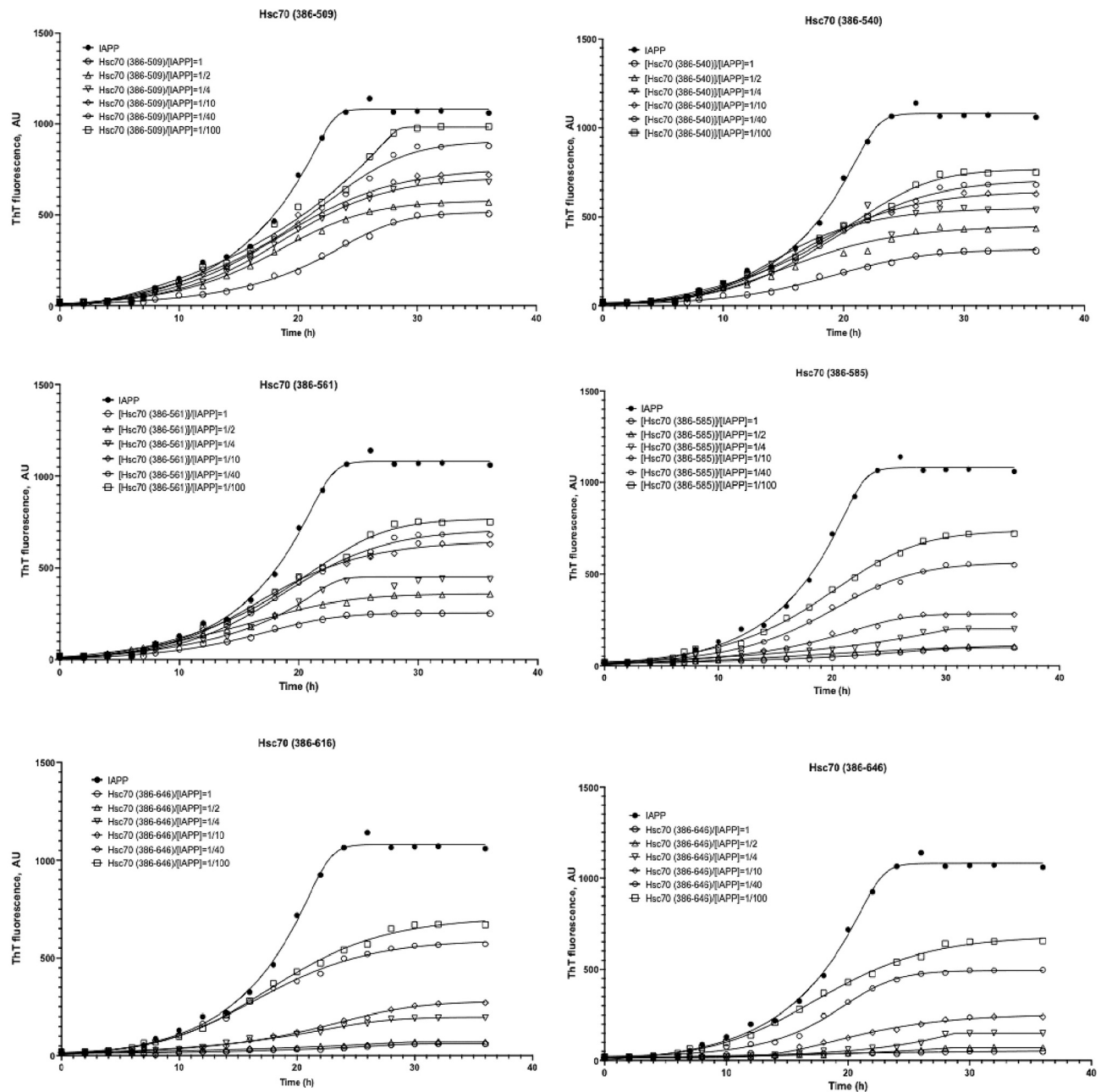


Fig. 4. The inhibition of hIAPP aggregation by structural domains of Hsc70.

A: The time dependence of hIAPP inhibition by structural domains of Hsc70. The time dependence of ThT fluorescence was fitted to a sigmoidal growth model. **B:** Percentage of Inhibition of hIAPP aggregation at a constant hIAPP concentration (15 μ M) and increasing concentrations of Hsc70 and its respective structural domains at 36 h of incubation. This inhibition was fitted using the hyperbolic eq. $Y = B_{\max} \cdot X / (K_d + X)$, where B_{\max} is the maximum specific binding in the same units as Y. It is the specific binding extrapolated to very high concentrations of [Hsc70], and so its value is almost always higher than any specific binding measured in the experiment. K_d is the equilibrium binding constant, in the same units as X. It is the chaperone concentration needed to achieve a half-maximum binding at equilibrium.

Hsc70 protein is 0.254 μ M, closely resembling that of the isolated C-terminal domain (0.256 μ M). It appears that eliminating the α -helices from the lid increases K_d (Table 1). Furthermore, the lag time, which denotes the time taken to achieve 10% of hIAPP aggregation's total fluorescence intensity with the isolated C-terminal domain (12.5 h), is roughly 40% longer than when devoid of the complete α -helices lid (7.5 h). A decline in the lag phase is also observed upon removal of the α -helices. Excising the full lid and retaining only the PBS (residues 386–509) compromises the activity of the SBD. This suggests that the subdomain (residues 510–646), excluding the EEVD, is crucial in

hindering hIAPP aggregation. Additionally, our findings suggest that the isolated C-terminal domain might reinforce its interaction with hIAPP's monomeric and minor aggregated forms, subsequently postponing the formation of seeds and fibrils.

3.4. Examining the delayed action of Hsc70 (386–646) on hIAPP aggregation

To understand how Hsc70 (386–646) affects the aggregation of hIAPP and whether its inhibitory effect depends on when it is introduced

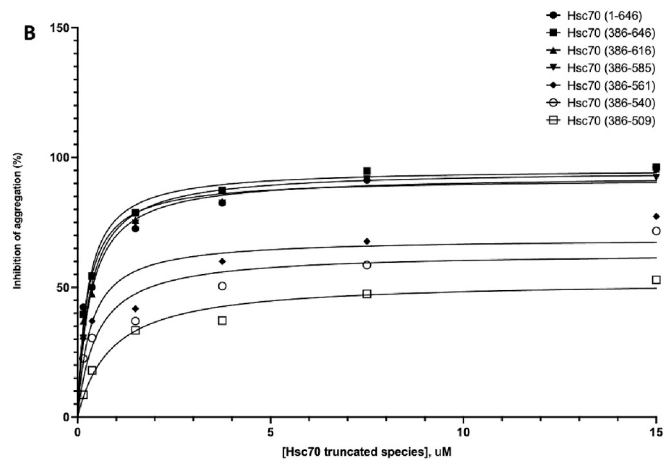


Fig. 4. (continued).

Table 1
Kinetic parameters of hIAPP aggregation in the presence and absence of Hsc70 and its structural domains as determined from fluorescence assays. The dissociation constant K_d is obtained from the hyperbolic eq. $Y = B_{max} * X / (K_d + X)$.

	T_{lag} (h)	Dissociation constant, μM
hIAPP	7	–
Hsc70 (1–646)	12	0.2537
Hsc70 (386–646)	12.5	0.2564
Hsc70 (386–616)	11	0.3187
Hsc70 (386–585)	10	0.3328
Hsc70 (386–561)	9	0.3358
Hsc70 (386–540)	8.2	0.5015
Hsc70 (386–509)	7.5	0.8719

during the aggregation process, we studied the impact of adding 15 μM of Hsc70 (386–646) to a 15 μM hIAPP solution at various stages of aggregation (Fig. 5). Specifically, we observed that the inhibitory effect of Hsc70 (386–646) is most pronounced when added early, before 8 h, corresponding to the lag phase, resulting in an inhibition rate of about 97%. If added at 18 h, amid the growth phase, the inhibition rate is 82%, while adding it at 22 h and 24 h results in inhibition rates of almost 11% and 3%, respectively. This suggests that Hsc70's inhibitory effect is most

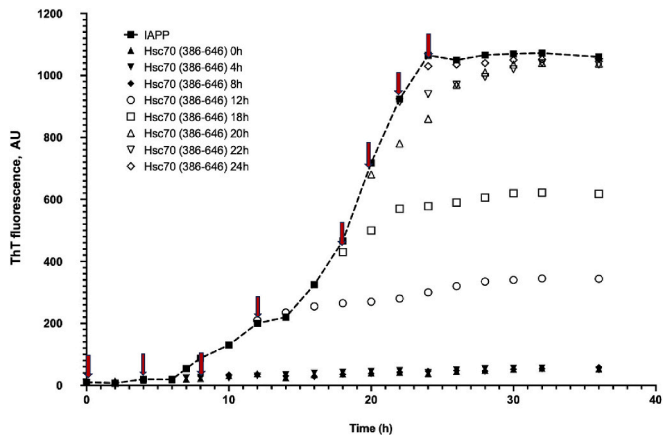


Fig. 5. Effect of Hsc70 (386–646) on different stages of hIAPP aggregation. 15 μM Hsc70 is added to a 15 μM hIAPP solution at different stages of aggregation (as pointed out by the red arrows), at the beginning ($t = 0$), ‘lag’ phase ($t = 4$ h and 8 h), at the beginning of the growth phase ($t = 12$ h and $t = 18$ h) and the second half of the growing phase ($t = 20$, $t = 22$ h, and $t = 24$ h, respectively). (For interpretation of the references to color in this figure legend, the reader is referred to the web version of this article.)

effective in the lag phase and diminishes as aggregation progresses, likely due to the irreversible formation of toxic polymers beyond a certain point [70].

When the chaperone is introduced during the prenucleation/nucleation phase, it delays hIAPP aggregation and slows down aggregate/fibril growth. However, if added during the post-nucleation phase when large aggregates/fibrils are already present (e.g., at $t = 20$ h, $t = 22$ h, and $t = 24$ h), it has no inhibitory effect, indicating that Hsc70 (386–646) may not modify the mature hIAPP's structural properties or cause fibrils to dissociate. The Hsc70 (386–646) appears to prevent the primary nucleation of hIAPP rather than inhibiting fibril growth, possibly through interactions with hIAPP monomers and small aggregates/prefibrillar oligomers. A similar mechanism of action of Hsp70 has been previously reported against early stages of tau aggregation in Alzheimer's disease [71].

3.5. Hsc70 abrogates hIAPP-induced cytotoxicity in INS-1E cells

One common feature in amyloid-related diseases is the misfolding or impaired clearance of potentially cytotoxic protein species [40,72]. Given that the C-terminal domains of Hsc70 (386–646) efficiently inhibit hIAPP aggregation, we were interested in assessing the cytotoxicity of the newly formed oligomers. We incubated hIAPP (15 μM), with or without 1.5 μM of Hsc70 (386–646), for 36 h. Samples were collected at different time points during incubation, and aggregation was analyzed using ThT assay (Fig. 6A). In parallel, cytotoxicity was assessed by MTT (Fig. 6B). ThT fluorescence revealed that oligomers obtained at different incubation times during the aggregation process exhibited varying degrees of cytotoxicity when added to the extracellular medium of INS-1E cells (Fig. 6B), confirming the previous report [47]. Small and medium hIAPP aggregates formed during the lag phase induced a significant reduction in cell viability by $66 \pm 5\%$ compared to the control sample or monomeric hIAPP solution. This aligns with the notion that amyloid proteins are more toxic in the early stages of aggregation [73]. However, when hIAPP samples incubated with C-terminal domains of Hsc70 (386–646) were added to the cells, cell survival increased (Fig. 6B), indicating that Hsc70 (386–646) mitigates the toxicity of hIAPP to INS-1E cells.

3.6. In silico study of Hsc70 structural domains and their impact on hIAPP aggregation

To further support our experimental findings and gain molecular insights into the binding of hIAPP to Hsc70 and its impact on hIAPP self-association, we conducted Discrete Molecular Dynamics (DMD) simulations. We explored the interaction between hIAPP monomers and

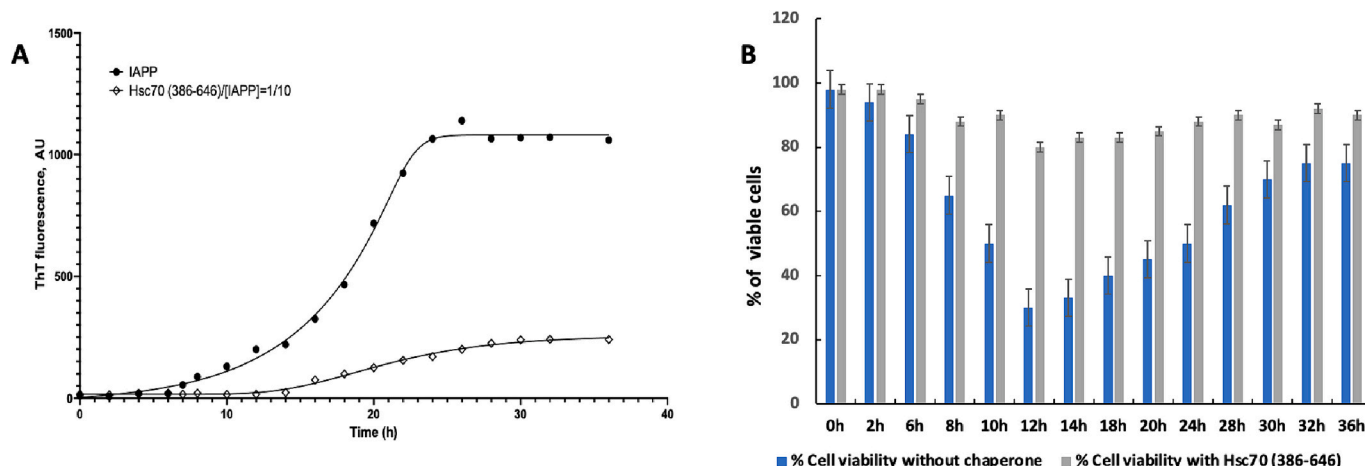


Fig. 6. Cell viability assays.

A: ThT fluorescence of hIAPP with or without incubation at 37 °C for 36 h.

B: Samples removed at different times of aggregation and added to INS-1E cells at 1 μ M final concentration of hIAPP with (grey line) or without (blue line). The values (average \pm S.D.) are obtained from three independent experiments. (For interpretation of the references to color in this figure legend, the reader is referred to the web version of this article.)

dimers with different structural variants of Hsc70: Hsc70- β -sandwich (385–509), Hsc70 + helix A (385–540), and Hsc70 + α -helices (385–615).

First, we performed a control MD simulation of the hIAPP monomer (Fig. S2), which demonstrated a predominance of a random coil conformation (coil content: 0.68) with a stable helical region between residues 8–16 (α -helix content: 0.21). Beta-sheet and turn regions constituted only a small fraction of the remaining secondary structure. Subsequently, we introduced the Hsc70- β -sandwich, known for its role in inhibiting aggregation, due to its experimentally established function as the PBSD. This domain possesses two exposed interfaces that could potentially interact with hIAPP monomers. This introduction resulted in a noteworthy increase in the residual β -sheet content, particularly around residues 15–20 and 24–32 (Fig. 7A).

This increase was attributed to the formation of interchain hydrogen bonds between hIAPP and the exposed β -strand edges of Hsc70- β -sandwich, specifically β 2 + β 3 and especially β 5 + β 8 (Fig. 7B and representative simulation snapshots). Per-residue binding probability calculations indicated that hydrophilic interactions played a significant role in stabilizing the interaction between hIAPP and Hsc70- β -sandwich, primarily around residues 11–29, including the amyloidogenic region. This stabilization was due to the propensity for extended β -sheet formation (Fig. 7C).

Considering that the combination of Hsc70- β -sandwich and helix A (Hsc70 + helix A, 385–540) exhibited greater inhibition than the β -sandwich alone in experimental studies, we further investigated their interaction with hIAPP monomers at the molecular level. The addition of helix A led to increased β -sheet content around residues 24–32, but the overall fractional residual β -sheet content in hIAPP reduced to 0.11 (compared to 0.14 with only the β -sandwich). Simultaneously, there was a corresponding increase in α -helix content (from 0.19 to 0.21), as shown in Fig. S3A. Importantly, we observed preferential binding to the β -strand edges along helix A (β 5 + β 8) with increased interchain hydrogen bonds (Fig. S3B). Per-residue binding probability studies confirmed the stronger binding of the hIAPP amyloidogenic region with Hsc70 + helix A, leading to an increased propensity to adopt β -sheet and α -helix structures (Fig. S3C). The addition of α -helix thus enhanced the binding interaction between hIAPP and Hsc70- β -sandwich, resulting in greater inhibition of aggregation compared to the β -sandwich alone, in line with the in vitro results. Experimentally, the addition of additional α -helices increased the lag time of aggregation and further inhibited hIAPP aggregation, likely due to their role in ATP-dependent regulation

of substrate binding and release.

To explore how the remaining α -helices affect inhibition at the molecular level, we simulated the interaction of hIAPP monomers with the entire helical lid subdomain (Hsc70 + α -helices, 385–615). We excluded the EEVD sequence as no co-chaperone was utilized, and it did not seem to contribute to aggregation inhibition even in in vitro experiments (Fig. 4B) [40]. Our simulations showed a reduction in hIAPP β -sheet content to 10% (from 14% with only the β -sandwich) and continued preferential binding to the β -strand edges along α -helices, with increased interchain hydrogen bonds as observed with helix A (Fig. 7D, E, and representative simulation snapshots). Per-residue binding studies yielded similar findings (Fig. 7F). These results demonstrate that the monomeric hIAPP binding to the Hsc70 chaperone disrupts protein-protein interactions. Ultimately, capping the exposed β -sheet edges of Hsc70- β -sandwich led to the inhibition of aggregation. While Hsc70- β -sandwich binding to hIAPP increased its residual β -sheet content, the presence of α -helices revealed an asymmetric binding of hIAPP to the two exposed edges of the β -sandwich. Moreover, our observations indicated that the amyloidogenic region of hIAPP preferentially binds to the Hsc70 chaperone, promoting β -sheet pairing and interchain hydrogen bonding in the complex.

Subsequently, we investigated how the mentioned Hsc70 mutants, namely β -sandwich and α -helices, interact with hIAPP dimers to understand if the addition of the chaperone at this stage within the aggregation cascade could still delay the process. Our findings showed that both β -sandwich and α -helices of Hsc70 mutants stabilized the binding around residues 11–29 of hIAPP through hydrophobic interactions. The amyloidogenic regions exhibited stronger binding to the chaperone, resulting in the formation of extended β -sheet structures. This increase in β -sheet content was particularly pronounced in the amyloidogenic binding regions, favoring the formation of extended β -sheets with the exposed edge of the β -sandwich and with the N-terminal of the chaperone (Fig. 8A and B). When complexed with β -sandwich, hIAPP predominantly formed anti-parallel β -sheets with β 8, β 3, and β 5 strands of Hsc70, with the strongest binding to β 5 and β 8 (Fig. 8C). The introduction of α -helices reduced the cross-linking of β -sheets on both exposed edges of the β -sandwich, with the substrate-binding domain (SBD) interface favoring stronger binding with hIAPP (Fig. 8D).

Similar to the monomeric hIAPP, the presence of both Hsc70 mutants led to reduced interchain hydrogen bonds (Fig. 8E) and reduced atomic contacts between hIAPP (Fig. 8F), suggesting that both chaperone

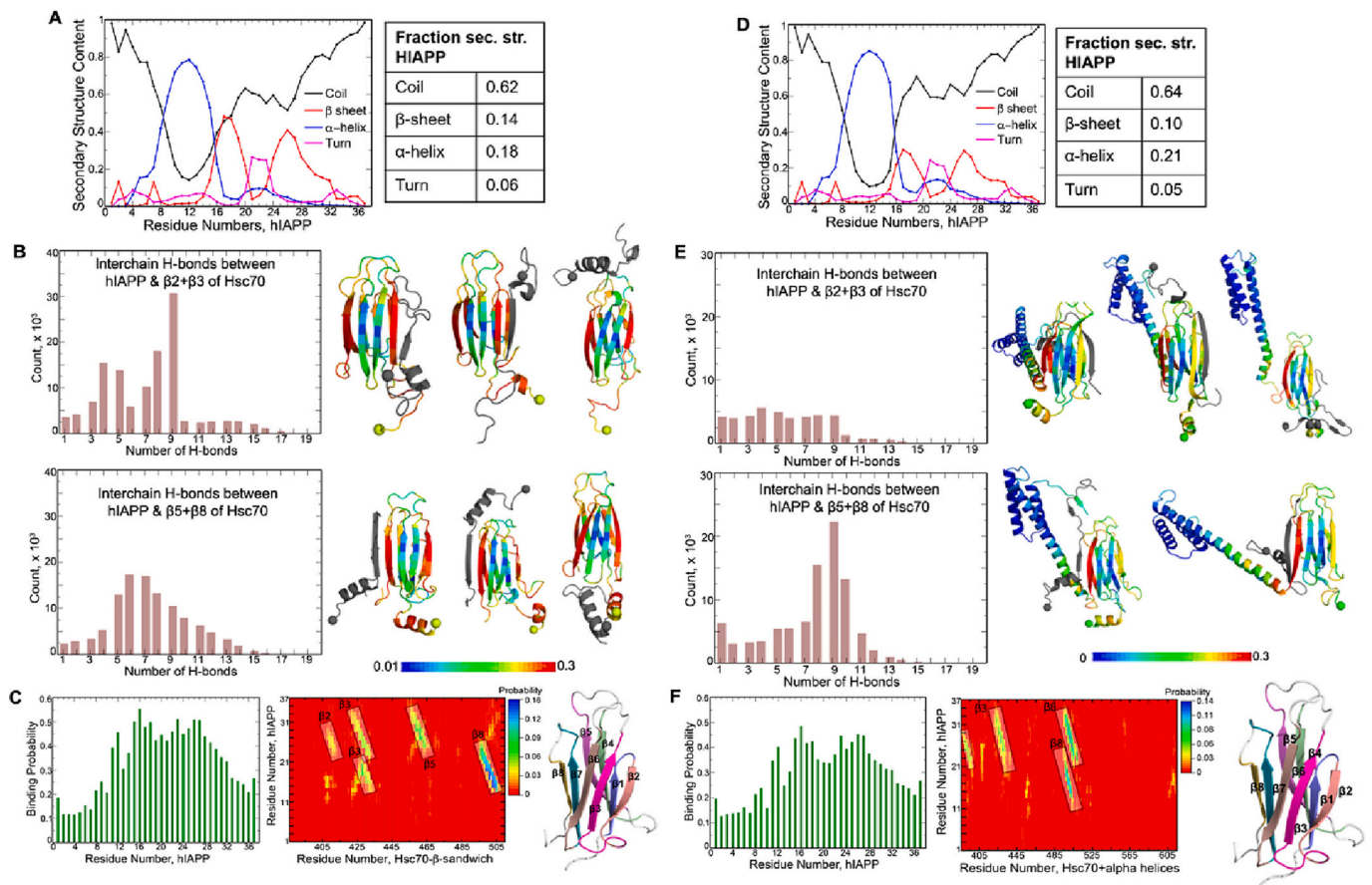


Fig. 7. DMD simulation of the interactions between hIAPP monomer and Hsc70-β-sandwich (A, B, C); and hIAPP monomer and Hsc70 + alpha helices (D, E, F). **A:** Residual secondary structure content corresponding to α-helix, β-sheet, random coil, and turn residues in hIAPP monomer. hIAPP shows stable helical regions around residues 8–16 and a significant increase in β-sheet content around residues 15–20 and 24–32. **B:** Number of interchain H-bonds formed between hIAPP and the two exposed β-strand edges of Hsc70-β-sandwich. hIAPP can directly bind to the two exposed β-strand edges of Hsc70-β-sandwich by forming interchain H-bonds and this interaction leads to an overall increase in residual β-sheet content in hIAPP. The representative structures show the binding of hIAPP to the two exposed β-strand edges along with binding to the N-terminal of the chaperone. The N-terminal residue is shown in sphere. The hot-spot regions of binding within the Hsc70-β-sandwich are color-coded according to the binding probability and the hIAPP monomer is colored in grey. **C:** Per-residue binding probability in hIAPP. Hydrophobic interactions mostly stabilize the binding to the β-sandwich around residues 11–29 of hIAPP. The amyloidogenic region has a stronger binding with Hsc70-β-sandwich which is also substantiated by the formation of an extended β-sheet. The residues with a high binding propensity to Hsc70 have strong probabilities of adopting β-sheet structures. The intermolecular contact frequency map between Hsc70 and hIAPP shows strong binding to the exposed edges. **D:** Residual secondary structure content in hIAPP monomer. hIAPP shows stable helical regions around residues 8–16 and an increase in β-sheet content in the amyloidogenic regions. In the presence of all alpha helices, the residual β-sheet content in hIAPP decreases to ~10%. **E:** Number of interchain H-bonds formed between hIAPP and the two exposed β-strand edges of Hsc70-β-sandwich. Similar to Hsc70 + helix A, hIAPP can directly bind to the two exposed β-strand edges by forming interchain H-bonds, however, binding to the β-strands along the alpha helices is preferred with increased interchain H-bonds. The representative structures highlight the binding of hIAPP to the two exposed β-strand edges along with alpha helices. The N-terminal residue is shown in sphere. The hot-spot regions of binding within Hsc70 + alpha helices are color-coded according to the binding probability and the hIAPP monomer is colored in grey. **F:** Per-residue binding probability in hIAPP. Hydrophobic interactions mostly stabilize the binding around residues 11–29 of hIAPP. The amyloidogenic region has stronger binding to the chaperone which leads to an extension in the β-sheet of hIAPP. The residues with a high binding propensity to Hsc70 have a higher probability of adopting β-sheet and α-helix structures.

mutants can inhibit intermolecular interactions between dimers. DMD simulations of hIAPP dimer and Hsc70 mutant complexes indicated the existence of a capping mechanism, which was favored along the substrate-binding interface. In the presence of Hsc70-β-sandwich and alpha-helices, hIAPP dimers exhibited reduced interchain hydrogen bonds, binding probability, and inter-chain atomic contacts, demonstrating their ability to reduce hIAPP aggregation. Notably, the alpha helices mutant exhibited unique conformational dynamics in the lid subdomain, which may facilitate hIAPP binding along the substrate-binding domain. The simulations suggest that Hsc70 (386–646) can delay hIAPP aggregation by interacting with hIAPP monomers and dimers, leading to the disruption of intermolecular interactions and the

formation of extended β-sheets.

4. Summary and conclusion

Misfolding of proteins is a key pathogenic factor in neurodegenerative and metabolic diseases [74]. Hsp70, a chaperone implicated in inhibiting hIAPP aggregation associated with Type 2 Diabetes, was investigated for its inhibitory effects on hIAPP aggregation through structural variants of Hsc70. We aimed to identify the optimal chaperone variant and elucidate the interaction mechanism. Remarkably, even at low concentrations, Hsc70 demonstrated a concentration-dependent hindrance of hIAPP aggregation. Notably, the ATPase

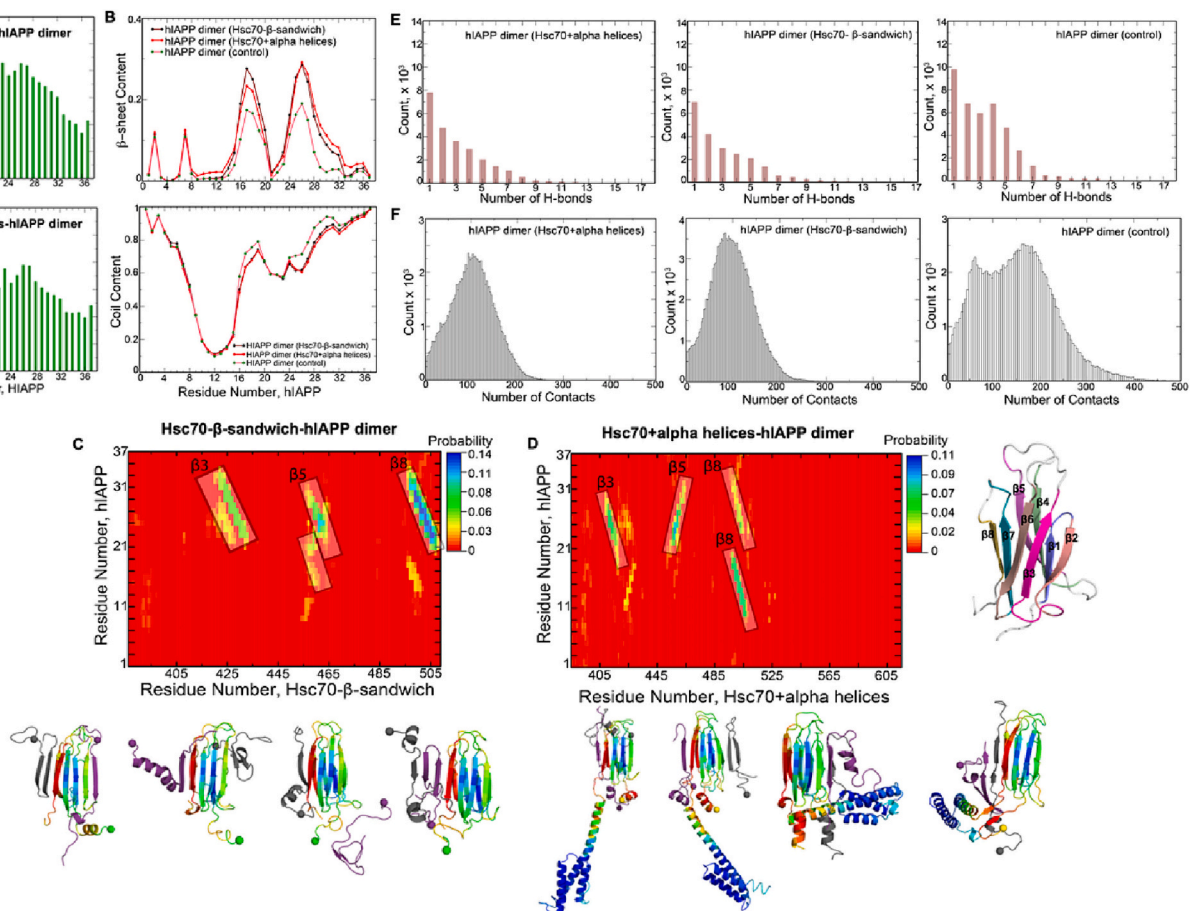


Fig. 8. Hsc70-β-sandwich with hIAPP dimer and Hsc70 + alpha helices with hIAPP dimer.

A: Per-residue binding probability of hIAPP dimer with Hsc70. Hydrophobic interactions mostly stabilize the binding around residues 11–29 of hIAPP. The amyloidogenic region exhibits stronger binding to the chaperone which leads to the formation of extended β-sheet in hIAPP.

B: Residual secondary structure content of hIAPP dimer with Hsc70. hIAPP shows an increase in the β-sheet content upon binding to Hsc70 chaperones compared to the control. The increase in the β-sheet content is prominent in the amyloidogenic binding regions of hIAPP which in turn favors the formation of extended β-sheets with the exposed edges of the β-sandwich and also with the N-terminal of the chaperone (see the representative structures). The N-terminal residue is shown in sphere. In the case of Hsc70-β-sandwich, the hIAPP dimer can bind on both sides of the exposed β-sheet edges, although one of the β-sheet edges has a higher probability for binding.

C: Intermolecular contact frequency map between Hsc70-β-sandwich and hIAPP. hIAPP forms anti-parallel β-sheets predominantly with β8, β3, and β5 strands of Hsc70. Stronger binding to β5 & β8 strands of the chaperone is predicted. The representative structures highlight hIAPP binding to the highlighted β-strands. The hot-spot regions of binding within the Hsc70-β-sandwich are color-coded according to the binding probability and hIAPP dimer is colored in grey and violet.

D: Intermolecular contact frequency map between Hsc70 + alpha helices and hIAPP. The presence of alpha helices reduces the cross-linking of β-sheets on both the exposed edges of the sandwich and the substrate binding domain interface favors stronger binding with hIAPP. hIAPP peptides can form either parallel or antiparallel β-sheets, which are stabilized by hydrophobic interactions. The color coding of representative structures is similar to that used in C.

E: Number of interchain H-bonds formed between hIAPP in the presence of Hsc70. The histogram of interchain H-bonds between hIAPP suggests the peptides to have reduced interchain H-bonds in the presence of the chaperone.

F: Per-residue number of atomic contacts between hIAPP. Similar to the observed trend in interchain H-bonds between hIAPP dimer, the interaction with Hsc70 chaperone reduces the atomic contacts between hIAPP. This suggests that the chaperone can inhibit intermolecular interactions between hIAPP dimer. (For interpretation of the references to color in this figure legend, the reader is referred to the web version of this article.)

activity of Hsc70 was dispensable, indicating a nucleotide-independent “holdase” mechanism, rather than a “foldase” mechanism. Subsequent investigations highlighted the pivotal role of the C-terminal substrate-binding domain of Hsc70, specifically the β-sandwich peptide-binding subdomain and the α-helical lid subdomain, in inhibiting hIAPP aggregation. Removal of the lid subdomain significantly attenuated the inhibitory effect of Hsc70, underscoring its overall importance.

In silico simulations employing hIAPP-Hsc70 complexes provided sub-atomic insights into interactions. The introduction of Hsc70-β-sandwich to hIAPP increased β-sheet content and facilitated interchain hydrogen bond formation. Conversely, the addition of the entire helical lid subdomain (Hsc70 + alpha helices) reduced hIAPP β-sheet content while maintaining preferential binding to alpha helices. Similar results were observed for Hsc70 mutants interacting with hIAPP dimers. In

summary, hIAPP binding to Hsc70 disrupted protein-protein interactions by shielding exposed β-sheet edges of Hsc70-β-sandwich, thereby preventing aggregation. These findings indicate that Hsc70 mutants effectively inhibit hIAPP aggregation by capping exposed β-sheet edges and disrupting protein interactions, with the alpha helices mutant displaying unique conformational dynamics, potentially facilitating hIAPP binding. Certainly, a conclusive affirmation awaits structural insights obtained from sophisticated techniques like AFM.

Combining in vitro and in silico data, we propose a comprehensive mechanism for Hsc70’s binding to hIAPP monomers and dimers (Fig. 9). This binding disrupts the uncontrolled growth of fibrils, thereby delaying the nucleation phase of hIAPP aggregation and inhibiting the formation and propagation of small soluble oligomers. Our study enhances the understanding of protein misfolding and provides valuable insights

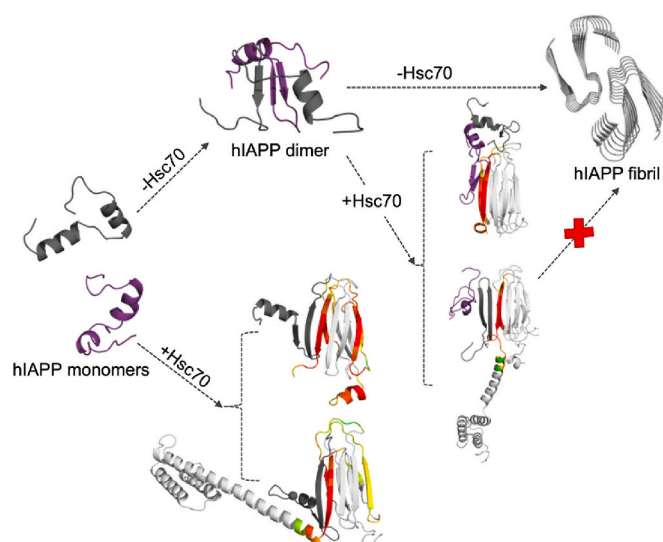


Fig. 9. The proposed mechanism of the binding of Hsc70 chaperone with hIAPP monomer and dimer.

hIAPP first forms dimer and higher-order oligomers by converting into β -sheet structures. Both Hsc70- β -sandwich and Hsc70 + α helices bind to the hIAPP monomer by forming intermolecular β -sheets with $\beta 3$ and $\beta 8$ strands of Hsc70 + α helices and β -sheets with $\beta 2$, $\beta 3$, $\beta 5$, and $\beta 8$ strands of Hsc70- β -sandwich. The exposed $\beta 2 + \beta 3$ and $\beta 5 + \beta 8$ edges of Hsc70 lead to favorable interaction with hIAPP. We propose that the binding of Hsc70 with hIAPP monomers and small aggregates (dimers) in the early stage of peptide aggregation is via β -sheet pairing that interrupts the continuous growth into long fibrils. In the presence of α helices, asymmetric binding of the two exposed edges of β -sandwich with hIAPP is revealed suggesting that the interaction is through a capping mechanism that can inhibit further fibril growth. Binding to $\beta 5 + \beta 8$ edges of Hsc70 along the α helix interface is preferred.

for potential targeted therapeutic strategies against diseases characterized by amyloid-related pathogenesis, including metabolic and neurodegenerative disorders.

CRediT authorship contribution statement

Ali Chaari: Writing – review & editing, Writing – original draft, Visualization, Validation, Supervision, Software, Resources, Project administration, Methodology, Investigation, Formal analysis, Data curation, Conceptualization. **Nabanita Saikia:** Writing – review & editing, Writing – original draft, Validation, Supervision, Software, Methodology, Investigation, Formal analysis, Data curation. **Pradipta Paul:** Writing – review & editing, Writing – original draft, Investigation, Data curation. **Mohammad Yousef:** Writing – review & editing, Formal analysis. **Feng Ding:** Writing – review & editing, Resources. **Moncef Ladjimi:** Writing – review & editing, Resources.

Declaration of competing interest

I hereby declare that all the mentioned information in the manuscript “Experimental and computational investigation of the effect of Hsc70 structural variants on inhibiting the amylin aggregation” are correct and accurate.

Appendix A. Supplementary data

Supplementary data to this article can be found online at <https://doi.org/10.1016/j.bpc.2024.107235>.

References

- [1] H. Sun, P. Saeedi, S. Karuranga, et al., IDF Diabetes Atlas: global, regional and country-level diabetes prevalence estimates for 2021 and projections for 2045, *Diabetes Res. Clin. Pract.* 183 (2022) 109119, <https://doi.org/10.1016/j.diabres.2021.109119>.
- [2] M.E. Cerf, Beta cell dysfunction and insulin resistance, *Front Endocrinol (Lausanne)*. 4 (2013) 37, <https://doi.org/10.3389/fendo.2013.00037>.
- [3] A.K. Bishoyi, P.H. Roham, K. Rachineni, et al., Human islet amyloid polypeptide (hIAPP) - a curse in type II diabetes mellitus: insights from structure and toxicity studies 402 (2) (2021) 133–153, <https://doi.org/10.1515/hsz-2020-0174>.
- [4] J.W.M. Höppener, C. Oosterwijk, M.G. Nieuwenhuis, et al., Extensive islet amyloid formation is induced by development of type II diabetes mellitus and contributes to its progression: pathogenesis of diabetes in a mouse model, *Diabetologia* 42 (4) (1999) 427–434, <https://doi.org/10.1007/s001250051175>.
- [5] C. Röcken, R.P. Linke, W. Saeger, Immunohistology of islet amyloid polypeptide in diabetes mellitus: semi-quantitative studies in a post-mortem series, *Virchows Arch. A Pathol. Anat. Histopathol.* 421 (4) (1992) 339–344, <https://doi.org/10.1007/BF01660981>.
- [6] A. Clark, C.A. Wells, I.D. Buley, et al., Islet amyloid, increased A-cells, reduced B-cells and exocrine fibrosis: quantitative changes in the pancreas in type 2 diabetes, *Diabetes Res.* 9 (4) (1988) 151–159.
- [7] P. Westermark, A. Andersson, G.T. Westermark, Islet amyloid polypeptide, islet amyloid, and diabetes mellitus, *Physiol. Rev.* 91 (3) (2011) 795–826, <https://doi.org/10.1152/physrev.00042.2009>.
- [8] T.D. O'Brien, P. Westermark, K.H. Johnson, Islet amyloid polypeptide and insulin secretion from isolated perfused pancreas of fed, fasted, glucose-treated, and dexamethasone-treated rats, *Diabetes* 40 (12) (1991) 1701–1706, <https://doi.org/10.2337/diab.40.12.1701>.
- [9] C.A. Jurgens, M.N. Toukatly, C.L. Fligner, et al., β -Cell loss and β -cell apoptosis in human type 2 diabetes are related to islet amyloid deposition, *Am. J. Pathol.* 178 (6) (2011) 2632–2640, <https://doi.org/10.1016/j.ajpath.2011.02.036>.
- [10] A.E. Butler, J. Janson, S. Bonner-Weir, R. Ritzel, R.A. Rizza, P.C. Butler, Beta-cell deficit and increased beta-cell apoptosis in humans with type 2 diabetes, *Diabetes* 52 (1) (2003) 102–110, <https://doi.org/10.2337/diabetes.52.1.102>.
- [11] S. Hassan, K. White, C. Terry, Linking hIAPP misfolding and aggregation with type 2 diabetes mellitus: a structural perspective, *Biosci. Rep.* 42 (5) (2022), <https://doi.org/10.1042/BSR20211297>.
- [12] D. Chatterjee Bhowmick, A. Jeremic, Functional proteasome complex is required for turnover of islet amyloid polypeptide in pancreatic β -cells, *J. Biol. Chem.* 293 (37) (2018) 14210–14223, <https://doi.org/10.1074/jbc.RA118.002414>.
- [13] S.B. Padrick, A.D. Miranker, Islet amyloid: phase partitioning and secondary nucleation are central to the mechanism of fibrillogenesis, *Biochemistry* 41 (14) (2002) 4694–4703, <https://doi.org/10.1021/bi0160462>.
- [14] B.W. Koo, A.D. Miranker, Contribution of the intrinsic disulfide to the assembly mechanism of islet amyloid, *Protein Sci.* 14 (1) (2005) 231–239, <https://doi.org/10.1110/ps.041051205>.
- [15] R. Kayed, J. Bernhagen, N. Greenfield, et al., Conformational transitions of islet amyloid polypeptide (IAPP) in amyloid formation in Vitro Edited by R. Huber, *J. Mol. Biol.* 287 (4) (1999) 781–796, <https://doi.org/10.1006/jmbi.1999.2646>.
- [16] L.E. Buchanan, E.B. Dunkelberger, H.Q. Tran, et al., Mechanism of IAPP amyloid fibril formation involves an intermediate with a transient β -sheet, *Proc. Natl. Acad. Sci. U. S. A.* 110 (48) (2013) 19285–19290, <https://doi.org/10.1073/pnas.1314481110>.
- [17] C. Betsholtz, L. Christmansson, U. Engström, et al., Sequence divergence in a specific region of islet amyloid polypeptide (IAPP) explains differences in islet amyloid formation between species, *FEBS Lett.* 251 (1–2) (1989) 261–264, [https://doi.org/10.1016/0014-5793\(89\)81467-x](https://doi.org/10.1016/0014-5793(89)81467-x).
- [18] P. Westermark, U. Engström, K.H. Johnson, G.T. Westermark, C. Betsholtz, Islet amyloid polypeptide: pinpointing amino acid residues linked to amyloid fibril formation, *Proc. Natl. Acad. Sci. U. S. A.* 87 (13) (1990) 5036–5040, <https://doi.org/10.1073/pnas.87.13.5036>.
- [19] S. Luca, W.-M. Yau, R. Leapman, R. Tycko, Peptide conformation and supramolecular organization in amylin fibrils: constraints from solid-state NMR, *Biochemistry* 46 (47) (2007) 13505–13522, <https://doi.org/10.1021/bi701427q>.
- [20] J. Zhang, J. Tan, R. Pei, S. Ye, Acidic environment significantly alters aggregation pathway of human islet amyloid polypeptide at negative lipid membrane, *Langmuir* 36 (6) (2020) 1530–1537, <https://doi.org/10.1021/acs.langmuir.9b03623>.
- [21] R. Akter, P. Cao, H. Noor, et al., Islet amyloid polypeptide: structure, function, and pathophysiology, *J. Diabetes Res.* 2016 (2016) 2798269, <https://doi.org/10.1155/2016/2798269>.
- [22] B.O.W. Elenbaas, S.M. Kreamreiter, L. Khemtoumian, J.A. Killian, T. Sinnige, Fibril elongation by human islet amyloid polypeptide is the main event linking aggregation to membrane damage, *BBA Adv.* 3 (2023) 100083, <https://doi.org/10.1016/j.bbadva.2023.100083>.
- [23] S. Asthana, B. Mallick, A.T. Alexandrescu, S. Jha, IAPP in type II diabetes: basic research on structure, molecular interactions, and disease mechanisms suggests potential intervention strategies, *Biochim. Biophys. Acta Biomembr.* 1860 (9) (2018) 1765–1782, <https://doi.org/10.1016/j.bbamem.2018.02.020>.
- [24] S.M. Ali, F. Nabi, M. Hisamuddin, et al., Evaluating the inhibitory potential of natural compound luteolin on human lysozyme fibrillation, *Int. J. Biol. Macromol.* 233 (2023) 123623, <https://doi.org/10.1016/j.ijbiomac.2023.123623>.
- [25] M.S. Fernández, Human IAPP amyloidogenic properties and pancreatic β -cell death, *Cell Calcium* 56 (5) (2014) 416–427, <https://doi.org/10.1016/j.cecc.2014.08.011>.

- [26] C. Huang, C. Lin, L. Haataja, et al., High expression rates of human islet amyloid polypeptide induce endoplasmic reticulum stress mediated beta-cell apoptosis, a characteristic of humans with type 2 but not type 1 diabetes, *Diabetes* 56 (8) (2007) 2016–2027, <https://doi.org/10.2337/db07-0197>.
- [27] S. Costes, C. Huang, T. Gurlo, et al., β -cell dysfunctional ERAD/ubiquitin/proteasome system in type 2 diabetes mediated by islet amyloid polypeptide-induced UCH-L1 deficiency, *Diabetes* 60 (1) (2011) 227–238, <https://doi.org/10.2337/db10-0522>.
- [28] S. Casas, R. Gomis, F.M. Gribble, J. Altirriba, S. Knuutila, A. Novials, Impairment of the ubiquitin-proteasome pathway is a downstream endoplasmic reticulum stress response induced by extracellular human islet amyloid polypeptide and contributes to pancreatic beta-cell apoptosis, *Diabetes* 56 (9) (2007) 2284–2294, <https://doi.org/10.2337/db07-0178>.
- [29] J.F. Rivera, T. Gurlo, M. Daval, et al., Human-IAPP disrupts the autophagy/lysosomal pathway in pancreatic β -cells: protective role of p62-positive cytoplasmic inclusions, *Cell Death Differ.* 18 (3) (2011) 415–426, <https://doi.org/10.1038/cdd.2010.111>.
- [30] G. Jing, C. Westwell-Roper, J. Chen, G. Xu, C.B. Verchere, A. Shalev, Thioredoxin-interacting protein promotes islet amyloid polypeptide expression through miR-124a and FoxA2 *, *J. Biol. Chem.* 289 (17) (2014) 11807–11815, <https://doi.org/10.1074/jbc.M113.525022>.
- [31] J.A. Corbett, Thioredoxin-interacting protein is killing my β -cells!, *Diabetes* 57 (4) (2008) 797–798.
- [32] A.V. Matveyenko, P.C. Butler, Beta-cell deficit due to increased apoptosis in the human islet amyloid polypeptide transgenic (HIP) rat recapitulates the metabolic defects present in type 2 diabetes, *Diabetes* 55 (7) (2006) 2106–2114, <https://doi.org/10.2337/db05-1672>.
- [33] S. Srodulski, S. Sharma, A.B. Bachstetter, et al., Neuroinflammation and neurologic deficits in diabetes linked to brain accumulation of amylin, *Mol. Neurodegener.* 9 (2014) 30, <https://doi.org/10.1186/1750-1326-9-30>.
- [34] K. Jackson, G.A. Barisone, E. Diaz, L. Jin, C. DeCarli, F. Despa, Amylin deposition in the brain: a second amyloid in Alzheimer disease? *Ann. Neurol.* 74 (4) (2013) 517–526, <https://doi.org/10.1002/ana.23956>.
- [35] H. Ly, N. Verma, F. Wu, et al., Brain microvascular injury and white matter disease provoked by diabetes-associated hyperamylinemia, *Ann. Neurol.* 82 (2) (2017) 208–222, <https://doi.org/10.1002/ana.24992>.
- [36] W. Gong, Z.H. Liu, C.H. Zeng, et al., Amylin deposition in the kidney of patients with diabetic nephropathy, *Kidney Int.* 72 (2) (2007) 213–218, <https://doi.org/10.1038/sj.ki.5002305>.
- [37] P. Arghavani, M. Pirhaghi, F. Moosavi-Movahedi, F. Mamashli, E. Hosseini, A. A. Moosavi-Movahedi, Amyloid management by chaperones: the mystery underlying protein oligomers' dual functions, *Curr Res Struct Biol.* 4 (2022) 356–364, <https://doi.org/10.1016/j.crsrbi.2022.11.002>.
- [38] R.A. Stetler, Y. Gan, W. Zhang, et al., Heat shock proteins: cellular and molecular mechanisms in the central nervous system, *Prog. Neurobiol.* 92 (2) (2010) 184–211, <https://doi.org/10.1016/j.pneurobio.2010.05.002>.
- [39] N. Chilukoti, T.B. Sil, B. Sahoo, et al., Hsp70 inhibits aggregation of IAPP by binding to the heterogeneous pre-nucleation oligomers, *Biophys. J.* 120 (3) (2021) 476–488, <https://doi.org/10.1016/j.bpj.2020.12.019>.
- [40] J. Tao, A. Berthet, Y.R. Citron, et al., Hsp70 chaperone blocks α -synuclein oligomer formation via a novel engagement mechanism, *J. Biol. Chem.* 296 (42) (2021) 1–2, <https://doi.org/10.1016/j.jbc.2021.100613>.
- [41] A. Chaari, D. Eliezer, M. Ladjimi, The C-terminal α -helices of mammalian Hsc70 play a critical role in the stabilization of α -synuclein binding and inhibition of aggregation, *Int. J. Biol. Macromol.* 83 (2016) 433–441, <https://doi.org/10.1016/j.ijbiomac.2015.10.089>.
- [42] Mouna Amor-Mahjoub, Nathalie Gomez-Vrielyunck, Jean Philippe Suppini, Benoit Fouchaq, Nadia Benaroudj, Moncef Ladjimi, Analysis of monomeric mutants of HSC70: a possible relationship between oligomerization and functional properties, *Protein Pept. Lett.* 14 (8) (2007) 761–765, <https://doi.org/10.2174/092986607781483624>.
- [43] M. Amor-Mahjoub, N. Gomez-Vrielyunck, J.P. Suppini, B. Fouchaq, N. Benaroudj, M. Ladjimi, Involvement of the interdomain hydrophobic linker and the C-terminal helices in self-association of the molecular chaperone HSC70, *Arch. Inst. Pasteur Tunis* 83 (1–4) (2006) 53–62, <https://doi.org/10.1021/bi060411d.PMID>.
- [44] M. Amor-Mahjoub, J.P. Suppini, N. Gomez-Vrielyunck, M. Ladjimi, The effect of the hexahistidine-tag in the oligomerization of HSC70 constructs, *J. Chromatogr. B Anal. Technol. Biomed. Life Sci.* 844 (2) (2006) 328–334, <https://doi.org/10.1016/j.jchromb.2006.07.031>.
- [45] O.H. Lowry, N.J. Rosebrough, A.L. Farr, R.J. Randall, Protein measurement with the Folin phenol reagent, *J. Biol. Chem.* 193 (1) (1951) 265–275, <http://www.ncbi.nlm.nih.gov/pubmed/14907713>.
- [46] S. Pemberton, K. Madiona, L. Pieri, M. Kabani, L. Bousset, R. Melki, Hsc70 protein interaction with soluble and fibrillar α -synuclein, *J. Biol. Chem.* 286 (40) (2011) 34690–34699, <https://doi.org/10.1074/jbc.M111.261321>.
- [47] A. Chaari, Inhibition of human islet amyloid polypeptide aggregation and cellular toxicity by oleuropein and derivatives from olive oil, *Int. J. Biol. Macromol.* 162 (2020) 284–300, <https://doi.org/10.1016/j.ijbiomac.2020.06.170>.
- [48] S. Pournourmohammadi, M. Grimaldi, M.H. Stridh, et al., Epigallocatechin-3-gallate (EGCG) activates AMPK through the inhibition of glutamate dehydrogenase in muscle and pancreatic β -cells: a potential beneficial effect in the pre-diabetic state? *Int. J. Biochem. Cell Biol.* 88 (2017) 220–225, <https://doi.org/10.1016/j.biocel.2017.01.012>.
- [49] A. Chaari, M. Ladjimi, Human islet amyloid polypeptide (hIAPP) aggregation in type 2 diabetes: correlation between intrinsic physicochemical properties of hIAPP aggregates and their cytotoxicity, *Int. J. Biol. Macromol.* 136 (2019) 57–65, <https://doi.org/10.1016/j.ijbiomac.2019.06.050>.
- [50] E.A. Proctor, N.V. Dokholyan, Applications of discrete molecular dynamics in biology and medicine, *Curr. Opin. Struct. Biol.* 37 (2016) 9–13, <https://doi.org/10.1016/j.sbi.2015.11.001>.
- [51] N. Benhamou Goldfajn, H. Tang, F. Ding, Substoichiometric inhibition of insulin against IAPP aggregation is attenuated by the incompletely processed N-terminus of proIAPP, *ACS Chem. Neurosci.* 13 (13) (2022) 2006–2016, <https://doi.org/10.1021/acscchemneuro.2c00231>.
- [52] N. Saikia, I.S. Yanez-Orozco, R. Qiu, et al., Integrative structural dynamics probing of the conformational heterogeneity in synaptosomal-associated protein 25, *Cell Rep. Phys. Sci.* 2 (11) (2021) 100616, <https://doi.org/10.1016/j.xcrp.2021.100616>.
- [53] G.L. Hamilton, N. Saikia, S. Basak, et al., Fuzzy supertertiary interactions within PSD-95 enable ligand binding. Kennedy MB, Dötsch V, Kennedy MB, Hendrix J, Lee A, eds, *Elife* 11 (2022), <https://doi.org/10.7554/eLife.77242> e77242.
- [54] N. Kolimi, A. Pabbathi, N. Saikia, F. Ding, H. Sanabria, J. Alper, Out-of-equilibrium biophysical chemistry: the case for multidimensional, integrated single-molecule approaches, *J. Phys. Chem. B* 125 (37) (2021) 10404–10418, <https://doi.org/10.1021/acs.jpcc.1c02424>.
- [55] J. Ma, N. Saikia, S. Godar, et al., Ensemble switching unveils a kinetic rheostat mechanism of the eukaryotic thiamine pyrophosphate riboswitch, *RNA* 27 (7) (2021) 771–790, <https://doi.org/10.1261/rna.075937.120>.
- [56] F. Ding, N.V. Dokholyan, in: N.V. Dokholyan (Ed.), *Discrete Molecular Dynamics Simulation of Biomolecules BT - Computational Modeling of Biological Systems: From Molecules to Pathways*, Springer US, 2012, pp. 55–73, https://doi.org/10.1007/978-1-4614-2146-7_3.
- [57] F. Ding, D. Tsao, H. Nie, N.V. Dokholyan, Ab initio folding of proteins with all-atom discrete molecular dynamics, *Structure* 16 (7) (2008) 1010–1018, <https://doi.org/10.1016/j.str.2008.03.013>.
- [58] T. Lazaridis, M. Karplus, Effective energy functions for protein structure prediction, *Curr. Opin. Struct. Biol.* 10 (2) (2000) 139–145, [https://doi.org/10.1016/S0959-440X\(00\)00063-4](https://doi.org/10.1016/S0959-440X(00)00063-4).
- [59] W. Kabsch, C. Sander, Dictionary of protein secondary structure: pattern recognition of hydrogen-bonded and geometrical features, *Biopolymers* 22 (12) (1983) 2577–2637, <https://doi.org/10.1002/bip.360221211>.
- [60] F. Chiti, C.M. Dobson, Protein misfolding, amyloid formation, and human disease: a summary of Progress over the last decade, *Annu. Rev. Biochem.* 86 (1) (2017) 27–68, <https://doi.org/10.1146/annurev-biochem-061516-045115>.
- [61] A. Mahboob, D.K.L. Senevirathne, P. Paul, F. Nabi, R.H. Khan, A. Chaari, An investigation into the potential action of polyphenols against human islet amyloid polypeptide aggregation in type 2 diabetes, *Int. J. Biol. Macromol.* (2022), <https://doi.org/10.1016/j.ijbiomac.2022.11.038>. Published online November 15.
- [62] Y. Bram, A. Frydman-Marom, I. Yanai, et al., Apoptosis induced by islet amyloid polypeptide soluble oligomers is neutralized by diabetes-associated specific antibodies, *Sci. Rep.* 4 (1) (2014) 4267, <https://doi.org/10.1038/srep04267>.
- [63] R. Qi, E.B. Sarbeng, Q. Liu, et al., Allosteric opening of the polypeptide-binding site when an Hsp70 binds ATP, *Nat. Struct. Mol. Biol.* 20 (7) (2013) 900–907, <https://doi.org/10.1038/nsmb.2583>.
- [64] C. Huang, H. Cheng, S. Hao, et al., Heat shock protein 70 inhibits α -synuclein fibril formation via interactions with diverse intermediates, *J. Mol. Biol.* 364 (3) (2006) 323–336, <https://doi.org/10.1016/j.jmb.2006.08.062>.
- [65] K.C. Luk, I.P. Mills, J.Q. Trojanowski, V.M.Y. Lee, Interactions between Hsp70 and the hydrophobic core of α -synuclein inhibit fibril assembly, *Biochemistry* 47 (47) (2008) 12614–12625, <https://doi.org/10.1021/bi801475r>.
- [66] S. Daturpalli, C.A. Waudby, S. Meenan, S.E. Jackson, Hsp90 inhibits α -synuclein aggregation by interacting with soluble oligomers, *J. Mol. Biol.* 425 (22) (2013) 4614–4628, <https://doi.org/10.1016/j.jmb.2013.08.006>.
- [67] A. Ciechanover, H. Heller, S. Elias, A.L. Haas, A. Hershko, ATP-dependent conjugation of reticulocyte proteins with the polypeptide required for protein degradation, *Proc. Natl. Acad. Sci. U. S. A.* 77 (3) (1980) 1365–1368, <https://doi.org/10.1073/pnas.77.3.1365>.
- [68] X. Zhu, X. Zhao, W.F. Burkholder, et al., Structural analysis of substrate binding by the molecular chaperone DnaK, *Science* (80-) 272 (5268) (1996) 1606–1614, <https://doi.org/10.1126/science.272.5268.1606>.
- [69] J. Cheng, T.J. Deming, Synthesis of polypeptides by ROP of NCAs, *Pept Mater.* 310 (June 2011) (2011) 1–26, <https://doi.org/10.1007/128>.
- [70] C. Mathieu, R.V. Pappu, J.P. Taylor, Beyond aggregation: pathological phase transitions in neurodegenerative disease, *Science* 370 (6512) (2020) 56–60, <https://doi.org/10.1126/science.abb8032>.
- [71] F. Kundel, S. De, P. Flagmeier, et al., Hsp70 inhibits the nucleation and elongation of tau and sequesters tau aggregates with high affinity, *ACS Chem. Biol.* 13 (3) (2018) 636–646, <https://doi.org/10.1021/acscchembio.7b01039>.
- [72] C.J. Huang, C.Y. Lin, L. Haataja, et al., High expression rates of human islet amyloid polypeptide induce endoplasmic reticulum stress-mediated β -cell apoptosis, a characteristic of humans with type 2 but not type 1 diabetes, *Diabetes* 56 (8) (2007) 2016–2027, <https://doi.org/10.2337/db07-0197>.
- [73] M. Stefani, C.M. Dobson, Protein aggregation and aggregate toxicity: new insights into protein folding, misfolding diseases and biological evolution, *J. Mol. Med.* 81 (11) (2003) 678–699, <https://doi.org/10.1007/s00109-003-0464-5>.
- [74] P. Paul, Z.R. Mahfoud, R.A. Malik, et al., Knowledge, awareness, and attitude of healthcare stakeholders on Alzheimer's disease and dementia in Qatar, *Int. J. Environ. Res. Public Health* 20 (5) (2023), <https://doi.org/10.3390/ijerph20054535>.